

Dark Photons in the Radio Sky: I. Resonant Conversions in Halos

Ethan Baker* and Hongwan Liu†

Physics Department, Boston University, Boston, MA 02215, USA

(Dated: November 14, 2025)

Mixing between dark photons and visible photons leads to substantial anisotropies in the cosmic microwave background due to resonant conversions of visible photons into dark photons in baryonic matter found in dark matter halos. In this *Letter*, we forecast the sensitivity of the Square Kilometre Array (SKA) to this signal. We find that SKA could be the first experiment to discover dark photons with a mass between 10^{-13} and 5×10^{-12} eV and kinetic mixing parameter ϵ as small as $\sim 10^{-8}$ by cross-correlating their data with a low-redshift galaxy survey, potentially improving on the sensitivity from a similar analysis using *Planck* data by a factor of 4 in ϵ . This improvement is largely due to an enhancement of the signal at low frequencies and the unique experimental advantages of radio telescopes such as small beam sizes. 

Introduction. — The dark photon A' is one of the simplest extensions to the Standard Model [1]. It is the gauge boson of a new dark $U(1)'$ symmetry, and couples to the Standard Model photon through a kinetic mixing term scaled by a mixing parameter ϵ , enabling $\gamma \leftrightarrow A'$ conversions. In a plasma, the probability of conversion is enhanced resonantly when the mass of the dark photon $m_{A'}$ is equal to the effective plasma mass m_γ , which is predominantly determined by the electron number density n_e in the gas. This effect allows for the search for $\gamma \leftrightarrow A'$ conversions in a variety of cosmological environments, with m_γ ranging from 10^{-15} eV– 10^{-5} eV. Here, we focus on $\gamma \rightarrow A'$ conversions, without assuming that dark photons are the dark matter.

Previous cosmological searches for $\gamma \rightarrow A'$ conversions have focused on the cosmic microwave background (CMB). Specifically, Refs. [2–8] set limits on the dark photon kinetic mixing parameter ϵ by searching for spectral distortions of the CMB monopole blackbody spectrum from such conversions. Refs. [4–6] found that properly modeling $\gamma \rightarrow A'$ conversions in the inhomogeneous plasma of our Universe was crucial to computing this spectral distortion signal accurately.

However, beyond just looking for the sky-averaged disappearance of CMB photons, we can also consider the angular power spectrum sourced by the inhomogeneous nature of $\gamma \rightarrow A'$ conversions [9–11]. This power spectrum of disappearing photons is determined by the cosmic distribution of free electrons, since $\gamma \rightarrow A'$ conversions occur when $m_{A'}^2 = m_\gamma^2 \propto n_e$. Using the halo model and a model for the distribution of baryons within a halo as a function of mass and redshift, Ref. [9] showed how to compute the photon disappearance angular power spectrum due to $\gamma \rightarrow A'$ in the gas within halos, as well as the cross-correlation of this signal with a galaxy catalog. Ref. [10] then performed an actual search for this signal using the *Planck* CMB temperature maps and the *unWISE* galaxy catalog, setting the strongest limits to

date on ϵ for $m_{A'} \sim 10^{-12}$ eV using the cross-correlation; this signal scales more favorably as ϵ^2 , compared to the auto-correlation signal, which scales as ϵ^4 .

In this *Letter*, we study for the first time $\gamma \rightarrow A'$ conversions at radio frequencies. We forecast the sensitivity of the Square Kilometre Array (SKA) to dark photons, and find that it will be one of the best ways to search for A' for two main reasons. First, the probability of $\gamma \rightarrow A'$ conversions occurring is proportional to ω^{-1} , where ω is the present-day photon energy, and is therefore enhanced by a factor of at least ~ 30 at radio frequencies compared to typical CMB frequencies. Second, radio telescopes like SKA operate with much smaller beams compared to *Planck*, giving radio telescopes much greater sensitivity to small angular scales, which is highly beneficial to searches for $\gamma \rightarrow A'$ conversions.

Our analysis is summarized in Fig. 1, and proceeds as follows:

1. *Modeling the dark photon signal.* We model $\gamma \rightarrow A'$ conversions in multiple cosmological environments using simulation and analytic methods, as detailed in our companion paper, Ref. [12] (hereafter **Paper II**), in order to be sensitive to the largest range of $m_{A'}$ possible. Here, for clarity, we focus on one representative case: $\gamma \rightarrow A'$ conversions in dark matter halos in the range $0.005 \leq z \leq 4$, which we model using the halo-model formalism of Refs. [9, 10]. We compute the angular auto-power spectrum of the temperature anisotropies sourced by $\gamma \rightarrow A'$ conversions, and its cross-power spectrum with the number density of low-redshift galaxies.
2. *Producing astrophysical foregrounds-only mock maps.* In order to forecast the sensitivity of SKA to a potential dark-photon signal, we produce 9 accurate, mock radio maps at 0.41 GHz–12.53 GHz containing only astrophysical foregrounds and experimental noise, corresponding to the null-signal hypothesis. The important foregrounds are galactic synchrotron radiation, free-free radiation, spinning dust, and extragalactic radio point sources [13–17].

* ebaker@bu.edu; ORCID: 0000-0002-0520-4235

† hongwan@bu.edu; ORCID: 0000-0003-2486-0681

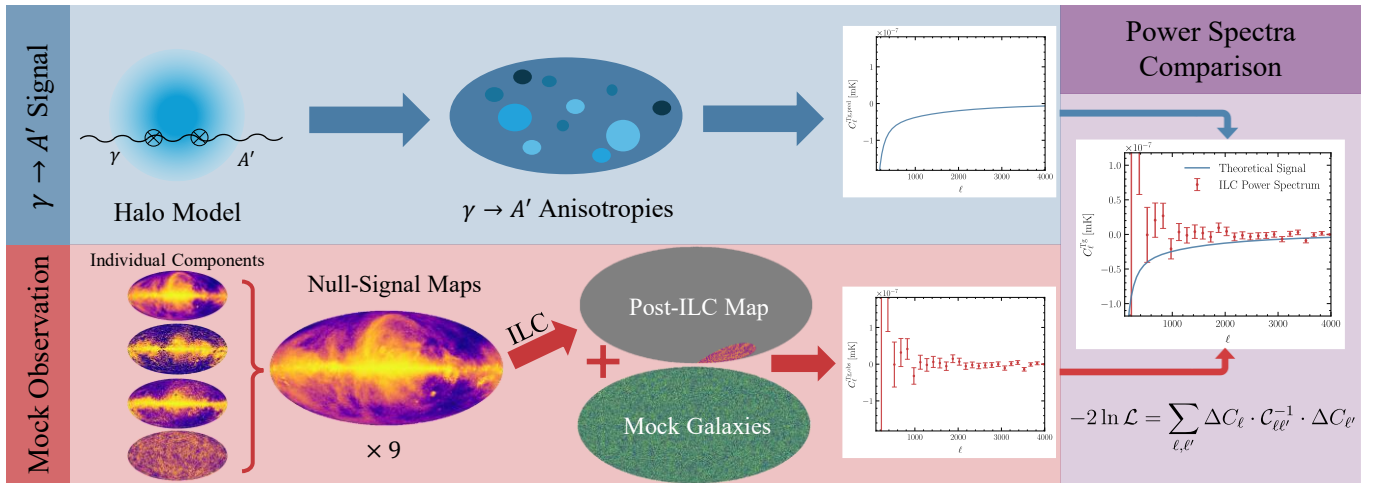


FIG. 1. A cartoon representation of the analysis pipeline. We begin with the theoretical prediction of the signal in the halo model. We then cross-correlate this predicted signal with a mock galaxy catalog to get a theoretical power spectrum. Next, we simulate astrophysical foregrounds to get 9 mock foreground maps at SKA frequencies, which we process with the ILC algorithm. Finally, this null-signal result is compared with the theory prediction using a Gaussian likelihood.

These mock foreground-only maps form the basis for our forecast analysis in the next step.

3. *Extracting a potential signal and likelihood analysis.*

Given any set of radio maps at different frequencies, we can optimally extract the putative dark-photon signal—with a known ω^{-1} frequency dependence—using a technique known as the internal linear combination (ILC) [18–21]. This algorithm constructs the minimum-variance linear combination of the input maps, subject to the constraint that the magnitude of the signal of interest is not reduced, given its known frequency dependence. In our analysis, we perform the ILC algorithm on the null-hypothesis maps, and compute the auto-power spectrum of the resulting post-ILC map as well as its cross-power spectrum with a mock galaxy survey. These power spectra are then compared with the theoretical signal to set an upper limit on the sensitivity of SKA to $\gamma \rightarrow A'$ conversions using a Gaussian likelihood constructed from these power spectra and the covariance of the post-ILC power spectrum.

In Paper II, we provide a detailed explanation of the dark photon signal, simulation techniques, foreground modeling, the ILC procedure, and statistical methods. In total, we consider three cosmological environments in which $\gamma \rightarrow A'$ conversions can occur: 1) conversions in dark matter halos, the focus of this *Letter*, 2) conversions in the intergalactic medium (IGM) during the Epoch of Reionization (EoR) from $5 \lesssim z \lesssim 35$, and 3) conversions in the late universe IGM from $0.005 \lesssim z \lesssim 4$. Additionally, we determine the sensitivity of 21-cm global signal experiments to $\gamma \rightarrow A'$ conversions. The remainder of this paper is structured as follows: First, we describe the general formalism of $\gamma \rightarrow A'$ conversions and the observational signals they generate. Next, we describe

our foreground modeling methods. We then forecast the sensitivity of upcoming radio experiments to $\gamma \rightarrow A'$ conversions and detail our important conclusions regarding the advantages of radio experiments. Throughout this work, we use natural units where $\hbar = c = k_B = 1$.

Radio Signals of $\gamma \rightarrow A'$ Conversions. — Photons and dark photons are described by the Lagrangian

$$\mathcal{L} \supset -\frac{1}{4}F_{\mu\nu}^2 - \frac{1}{4}F'_{\mu\nu}{}^2 - \frac{\epsilon}{2}F^{\mu\nu}F'_{\mu\nu} + \frac{1}{2}m_{A'}^2 A_\mu'^2, \quad (1)$$

where $m_{A'}$ is the dark photon mass and ϵ is the kinetic mixing parameter that controls the strength of the interaction [1]. The kinetic mixing term causes $\gamma \leftrightarrow A'$ oscillations. In a plasma, the probability of these conversions is enhanced resonantly when $m_{A'}^2$ equals the effective plasma mass $m_\gamma^2(\vec{x}) \approx 4\pi\alpha_{\text{EM}}n_e(\vec{x})/m_e$, where α_{EM} is the electromagnetic fine structure constant, n_e is the free electron number density, and m_e is the electron mass.

The total probability of conversion along a line-of-sight \hat{n} is given by a sum over all conversions as a photon travels from the last scattering surface to us,

$$P_{\gamma \rightarrow A'}(\hat{n}) = \sum_i \frac{\pi\epsilon^2 m_{A'}^2}{H(z_i)\omega_0(1+z_i)^2} \left| \frac{d \ln m_\gamma^2(\hat{n}, z)}{dz} \right|_{z=z_i}^{-1}, \quad (2)$$

where $H(z)$ is the Hubble parameter, z_i are the redshifts when resonances occur and ω_0 is the present-day energy of the photon [2, 5].

These conversions reduce the specific intensity in frequency of the incoming isotropic backlight photons from the CMB along a line of sight by $\Delta I(\omega_0, \hat{n}) = -P_{\gamma \rightarrow A'} B(\omega_0)$, where

$$B(\omega_0) = \frac{\omega_0^3}{2\pi^2} \left[\exp\left(\frac{\omega_0}{T_{\gamma,0}}\right) - 1 \right]^{-1} \quad (3)$$

and $T_{\gamma,0} = 2.73$ K is the present-day temperature of the CMB [22]. This corresponds to a thermodynamic temperature deficit $\Delta T(\hat{n}) = -P_{\gamma \rightarrow A'}(\omega_0, \hat{n})T_{\gamma,0}(1 - e^{-x})/x$ with $x \equiv \omega_0/T_{\gamma,0}$. At the radio frequencies of interest here, this simplifies to $\Delta T(\hat{n}) \approx -T_{\gamma,0}P_{\gamma \rightarrow A'}(\omega_0, \hat{n})$; at frequencies above $T_{\gamma,0}$, however, the temperature deficit is exponentially suppressed.

To search for this disappearance signal, we begin by constructing two real-space summary statistics: the two-point auto-correlation function ξ^{TT} of ΔT , and the two-point cross-correlation function ξ^{Tg} of ΔT and the sky-projected fractional overdensity of galaxies, δ_g , defined as:

$$\begin{aligned}\xi^{\text{TT}}(\mu) &\equiv \langle \Delta T(\hat{n})\Delta T(\hat{n}') \rangle - \langle \Delta T \rangle^2, \\ \xi^{\text{Tg}}(\mu) &\equiv \langle \Delta T(\hat{n})\delta_g(\hat{n}') \rangle - \langle \Delta T(\hat{n}) \delta_g(\hat{n}) \rangle,\end{aligned}\quad (4)$$

where $\langle \dots \rangle$ indicates the sky average, and $\mu \equiv \hat{n} \cdot \hat{n}'$. We can then define the corresponding angular power spectra,

$$C_\ell^{\text{TX}} = 2\pi \int_{-1}^1 d\mu \xi^{\text{TX}}(\mu) P_\ell(\mu), \quad (5)$$

where $X \in \{\text{T}, \text{g}\}$ and P_ℓ is a Legendre polynomial. Note that we have assumed isotropy throughout these expressions. These are the main observables of interest in this *Letter*; we will perform our forecast of SKA's sensitivity to dark-photon conversions by comparing the theoretical predictions of these power spectra, $C_\ell^{\text{TX,pred}}$, to $C_\ell^{\text{TX,obs}}$ obtained from mock data.

$C_\ell^{\text{TX,pred}}$ are computed by adopting the methods from Ref. [10], described in more detail in Paper II. In summary, we first adopt a halo model, which specifies the number density of halos as a function of their mass and redshift. Each halo within the distribution is then assigned a baryon distribution from Ref. [23]. With this, we know how $\gamma \rightarrow A'$ conversions should proceed within the gas of each halo. Furthermore, the halo model, together with the halo occupation distribution model from Ref. [24], also predicts the distribution of galaxies in the sky. Combining all of this information, we can compute first the two-point correlation functions in Eq. (4), and then subsequently $C_\ell^{\text{TX,pred}}$. Representative cases of $C_\ell^{\text{TT,pred}}$ and $C_\ell^{\text{Tg,pred}}$ computed in the halo model are shown as black lines in Fig. 2 for $m_{A'} = 5.6 \times 10^{-13}$ eV at $\omega_0/(2\pi) = 410$ MHz.

Mock Foreground & Galaxy Modeling. — In order to perform a forecast for SKA, we need to produce foreground-only maps, which correspond to the null-hypothesis that there is no dark-photon signal. The forecast upper limits on ϵ will then be set by processing these maps with the same pipeline that would be used for real SKA data, computing $C_\ell^{\text{TX,obs}}$ for these maps, and comparing to the theoretical predictions, $C_\ell^{\text{TX,pred}}$. In this section, we describe our methods for modeling astrophysical foregrounds and producing a mock galaxy catalog that we will then use to forecast the sensitivity of SKA. The details of our modeling are described in Paper II.

First, we generate 9 mock foreground-only maps in the HEALPix format [25] with $N_{\text{side}} = 2048$ at the SKA observing band centers: $\{0.41, 0.56, 0.77, 1.05, 1.43, 4.94, 6.74, 9.19, 12.53\}$ GHz [26]. There are four dominant sources of astrophysical foregrounds: galactic synchrotron radiation, galactic free-free radiation, spinning dust, and extragalactic point sources [27]. We simulate the first three foregrounds using the PYSM3 code [13–15] and the point sources using EPSKY [17]. These foregrounds are simulated by beginning with template maps like the 408 MHz Haslam map from Ref. [28] and WMAP data [29]. Then, small scale features are added to these templates under the standard assumption that C_ℓ obeys a power law at high- ℓ for each foreground. We assume that point sources brighter than $S_{\text{max}} = 0.1$ mJy can be masked and are not a significant foreground; this choice is comparable to the threshold at LOFAR [30], which SKA should outperform. Given the extremely small SKA beams [26], we account for this masking by excluding these resolved sources from our mock foreground map [31, 32]. However, a diffuse background of unresolved sources remains, which we model by using fits to their number density per unit flux, and their two-point correlation functions [16, 17, 33, 34].

Besides astrophysical foregrounds, we also add thermal noise to each map, which is drawn in each pixel from a Gaussian with $\sigma_{\text{rms}} = 7.25 \mu\text{Jy beam}^{-1}$ [30], which is greater than the expected thermal noise after 10 hours of observing at SKA [26]. We then mask the mock foreground maps, leaving only a 20° patch in the Southern Hemisphere unmasked, which greatly reduces the impact of galactic foregrounds.

Additionally, we also produce a mock map of δ_g that we cross-correlate with the $\gamma \rightarrow A'$ signal, constructed from the power spectrum of galaxies obtained from an HOD that is fit to the *unWISE* galaxy survey [24].

ILC Pipeline. — Now that we have modeled the mock null-hypothesis maps, we analyze them with the needlet ILC algorithm [20] that would be used to extract the $\gamma \rightarrow A'$ signal from the real SKA maps. At radio frequencies, variations of this algorithm have also been proposed to search for the cosmological 21-cm signal [35–37].

The needlet ILC constructs the minimum-variance linear combination of our 9 mock maps without reducing the strength of the dark-photon signal of interest, which has frequency dependence $\propto \omega^{-1}$. We perform the needlet ILC algorithm using PYILC [21] (see Paper II for more details.) The end product of this process is a single map, which is the optimal weighted sum of the input maps. We choose the normalization of the resulting map to be the magnitude of a signal-only map at $\omega_0/(2\pi) = 410$ MHz. We run the ILC pipeline on our mock null-signal maps to obtain a post-ILC map, from which we compute the auto- and cross-power spectrum (with the mock δ_g map), $C_\ell^{\text{TT,obs}}$ and $C_\ell^{\text{Tg,obs}}$ respectively. These are shown in Fig. 2 in orange, labeled “fiducial”, and can be compared to several representative plots of $C_\ell^{\text{TX,pred}}$ to get a sense of the sensitivity of SKA to dark photons.

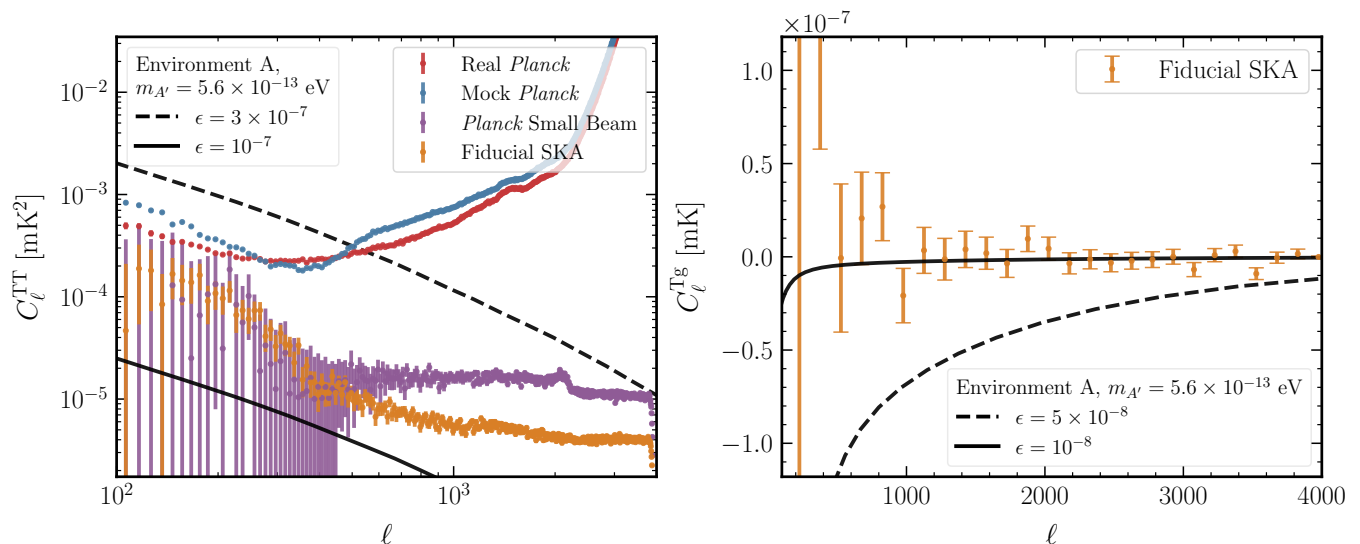


FIG. 2. The power spectra of several post-ILC maps compared to the theoretical signal. (*Left*): The red and blue lines are the auto-power spectra from performing the ILC procedure on real and mock *Planck* maps at the actual beams, respectively. The orange and purple lines are the auto-power spectra of our post-ILC fiducial mock radio and mock *Planck* maps, respectively, with a $0.5'$ beam. (*Right*): The cross-power spectra of our fiducial post-ILC map with our mock δ_g is compared to the theoretical dark photon signal. In both plots, the theoretical signal (in black) is for a dark photon with $m_{A'} = 5.6 \times 10^{-13}$ eV. \odot

To validate our entire analysis procedure, we compare our results to previous work in the CMB frequency range. First, we apply our ILC pipeline to the PR4 NPIPE *Planck* maps [38] used in Refs. [10, 21, 39] to obtain a post-ILC C_ℓ^{TT} angular power spectrum, shown in red in Fig. 2. This power spectrum agrees well with Fig. 1 of Ref. [10], validating the ILC procedure. Next, we use the pipeline to produce mock maps at the *Planck* frequencies and beam sizes. These *Planck* mock maps are then processed with our pipeline, and the resulting power spectrum is shown in blue in Fig. 2. This mock power spectrum agrees relatively well with the actual *Planck* power spectrum, demonstrating that our foreground modeling is able to accurately reproduce the *Planck* sky.

Sensitivity of Radio Experiments. — To estimate the sensitivity of SKA to the dark-photon signal, we construct a Gaussian likelihood of the form

$$-2 \ln \mathcal{L}_{\text{TX}}(\epsilon) = \sum_{\ell, \ell'} \Delta C_\ell^{\text{TX}} \cdot C_{\ell\ell'}^{-1} \cdot \Delta C_{\ell'}^{\text{TX}}, \quad (6)$$

where $\Delta C_\ell^{\text{TX}} \equiv C_\ell^{\text{TX, pred}} - C_\ell^{\text{TX, obs}}$, for $X = \{T, g\}$. All C_ℓ 's are binned with width $\Delta\ell = 150$. $C_{\ell\ell'}$ is the Gaussian covariance between each ℓ bin, which we compute assuming Gaussian statistics with PYMASTER to account for mask effects [40–42]. We use these likelihoods to find the 95% confidence upper limit for ϵ , which are shown in Fig. 3 for the full range of models and experiments that we consider in Paper II.

Overall, we find that radio experiments will have strong sensitivity to dark photon conversions for the models that we consider. The sensitivity is greatest for the analysis that we focus on in the *Letter*, i.e. when

considering the cross-correlation between $\gamma \rightarrow A'$ conversions in dark matter halos and low-redshift galaxies for 10^{-13} eV $\lesssim m_{A'} \lesssim 5 \times 10^{-12}$ eV, shown as the red solid line in Fig. 3. SKA is sensitive to $\epsilon \sim 10^{-8}$ over this mass range, a factor of up to 4 improvement compared to the *Planck* limit.

This improvement in sensitivity is due to two reasons. First, since the probability of conversion is proportional to ω^{-1} , the signal is enhanced relative to CMB frequencies. Furthermore, since $\Delta T \propto x^{-1}(1 - e^{-x})P_{\gamma \rightarrow A'}$, the observable signal at radio experiments does not suffer the exponential suppression that occurs at the high end of the CMB frequencies.

Second, the smaller beams used in radio experiments drastically improve sensitivity. The auto-power spectrum of the post-ILC maps constructed from *Planck* data (Fig. 2, red) become large at high ℓ , owing to the finite beam width of *Planck*. At the lowest frequencies, the *Planck* beams have a full-width half-maximum of $\theta_{\text{FWHM}} \approx 30'$, leading to an exponential suppression of power in the maps at angular scales corresponding to $\ell \gtrsim 300$. In terms of the $\gamma \rightarrow A'$ signal, this means that the information used in the ILC procedure at large- ℓ comes from the high frequency maps; these have smaller beams, but also a weaker signal, leading to a loss in sensitivity and larger $C_\ell^{\text{TT, obs}}$ at high- ℓ .

To confirm this interpretation, we compare our fiducial (Fig. 2, orange) post-ILC C_ℓ^{TT} to the post-ILC C_ℓ^{TT} that we would obtain at *Planck* frequencies, but with a much smaller beam of $\theta_{\text{FWHM}} = 0.5'$, comparable to the SKA beam size (Fig. 2, purple). We find a significantly smaller post-ILC C_ℓ^{TT} at high- ℓ with the smaller beam,

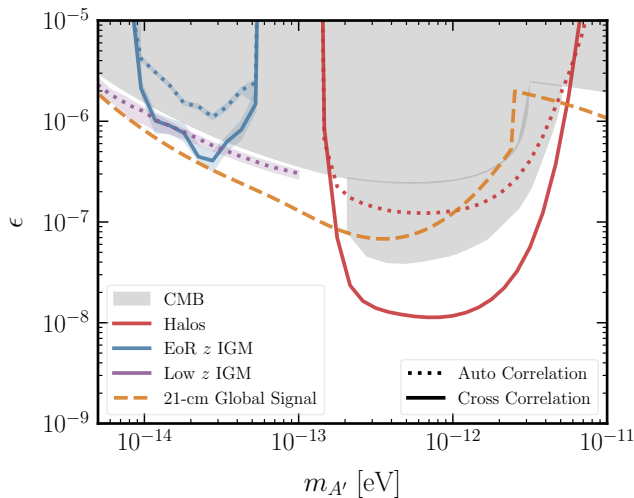


FIG. 3. Our forecasted sensitivity for a future radio search for dark photons. Shown are the sensitivities from modeling $\gamma \rightarrow A'$ conversions in dark matter halos and $\gamma \rightarrow A'$ conversions in the IGM during the EoR. The band around the EoR IGM limits shows the uncertainty in our inferred limits. In both cases, we show the sensitivities from considering auto-correlations and cross-correlations with the relevant galaxy survey. Also shown is the expected sensitivity of a 21-cm global signal experiment to $\gamma \rightarrow A'$ conversions and our rudimentary estimate of the auto-correlation signal from conversions in the late universe IGM. \odot

demonstrating that the loss of sensitivity with *Planck* at high- ℓ is due to the wide *Planck* beams.

Discussion. — In Fig. 3 we plot the sensitivity of SKA and 21-cm global signal experiments to dark photon conversions in the IGM, which we discuss in detail in Paper II. We first find that that SKA cross-correlated with high-redshift galaxies survey will be slightly more sensitive to dark photons than limits from CMB spectral distortions [4]. We compute this sensitivity by modeling $\gamma \rightarrow A'$ conversions in the IGM during the EoR and a catalog of high-redshift galaxies using the semi-analytic code 21CMFAST [43–45]. We also estimate the sensitivity of SKA to $\gamma \rightarrow A'$ conversions that occur in the late universe IGM, assuming that the baryon number density is distributed according to a lognormal distribution. Al-

though this is a crude model, we predict a strong $\gamma \rightarrow A'$ signal, motivating a more sophisticated hydrodynamical simulation study.

Beyond these imaging experiments, we further examine the sensitivity of 21-cm experiments to $\gamma \rightarrow A'$ conversions in Paper II. We find that a 21-cm global signal experiment is highly sensitive to $\gamma \rightarrow A'$ conversions if it can be disentangled from other foregrounds, but that the experimental details of a power spectrum experiment complicate the prospects for carrying out such a search there.

We note that a study with actual data must consider several additional points. In particular, Ref. [10] showed that the ILC can be slightly biased by foregrounds correlated with the $\gamma \rightarrow A'$ signal; such components must be explicitly deprojected. We have not included this correction here, but based on the results of Ref. [10], we expect only a modest weakening our projected sensitivities. Additionally, we have not accounted for a possible correlation between extragalactic radio emission and a galaxy survey. This correlation could produce a non-zero positive cross-correlation between the ILC map and a galaxy survey, which would artificially strengthen SKA’s sensitivity. Simulating this correlation is beyond the scope of this work, but Ref. [10] demonstrated that this bias mostly impacts large angular scales, and can be successfully subtracted. We anticipate that a similar subtraction procedure would be effective in our analysis, but certainly a more detailed study is warranted with actual data.

Acknowledgements. — We would like to thank Colin Hill, Junwu Huang, Cristina Mondino and Julian Muñoz for helpful conversations. The work in this paper make extensive use of the NUMPY [46], SCIPY [47], MATPLOTLIB [48], ASTROPY [49–51], HALOMOD [52, 53], HEALPY, and HEALPIX packages [54, 55]. We are also pleased to acknowledge that the computational work reported on in this paper was performed on the Shared Computing Cluster which is administered by Boston University’s Research Computing Services. EB was supported by the Boston University Dean’s Fellowship program. EB and HL are supported by the U.S. Department of Energy under grant DE-SC0026297 and the Cecile K. Dalton Career Development Professorship, endowed by Boston University trustee Nathaniel Dalton and Amy Gottlieb Dalton.

-
- [1] B. Holdom, *Physics Letters B* **166**, 196 (1986).
 - [2] A. Mirizzi, J. Redondo, and G. Sigl, *Journal of Cosmology and Astroparticle Physics* **2009** (03), 026.
 - [3] K. E. Kunze and M. A. Vazquez-Mozo, *Journal of Cosmology and Astroparticle Physics* **2015** (12), 028, arXiv:1507.02614 [astro-ph, physics:hep-ph].
 - [4] A. Caputo, H. Liu, S. Mishra-Sharma, and J. T. Ruder- man, *Physical Review Letters* **125**, 221303 (2020).
 - [5] A. Caputo, H. Liu, S. Mishra-Sharma, and J. T. Ruder- man, *Physical Review D* **102**, 103533 (2020).
 - [6] A. A. Garcia, K. Bondarenko, S. Ploekinger, J. Pradler, and A. Sokolenko, *JCAP* **10**, 011.
 - [7] J. Chluba, B. Cyr, and M. C. Johnson, *Mon. Not. Roy. Astron. Soc.* **535**, 1874 (2024).
 - [8] G. Arsenadze, A. Caputo, X. Gan, H. Liu, and J. T. Ruder- man, *JHEP* **03**, 018.
 - [9] D. Pirvu, J. Huang, and M. C. Johnson, *Journal of Cos- mology and Astroparticle Physics* **2024** (01), 019.
 - [10] F. McCarthy, D. Pirvu, J. C. Hill, J. Huang, M. C. John- son, and K. K. Rogers, *Phys. Rev. Lett.* **133**, 141003

- (2024).
- [11] A. Aramburo-Garcia, K. Bondarenko, A. Boyarsky, P. Kashko, J. Pradler, A. Sokolenko, R. Kugel, M. Schaller, and J. Schaye, *JCAP* **11**, 049.
- [12] E. Baker and H. Liu, Dark Photons in the Radio Sky: II. Resonant Conversions in the Intergalactic Medium.
- [13] B. Thorne, J. Dunkley, D. Alonso, and S. Naess, *Monthly Notices of the Royal Astronomical Society* **469**, 2821 (2017), arXiv:1608.02841 [astro-ph].
- [14] A. Zonca, B. Thorne, N. Krachmalnicoff, and J. Borrill, *Journal of Open Source Software* **6**, 3783 (2021), arXiv:2108.01444 [astro-ph].
- [15] J. Borrill *et al.* (The Pan-Experiment Galactic Science Group), Full-sky Models of Galactic Microwave Emission and Polarization at Sub-arcminute Scales for the Python Sky Model (2025).
- [16] M. Gervasi, A. Tartari, M. Zannoni, G. Boella, and G. Sironi, *Astrophys. J.* **682**, 223 (2008).
- [17] S. Mittal, G. Kulkarni, D. Anstey, and E. de Lera Acedo, *Monthly Notices of the Royal Astronomical Society* **534**, 1317 (2024).
- [18] C. Bennett *et al.* (WMAP Collaboration), *Astrophys. J. Suppl.* **148**, 97 (2003).
- [19] M. Tegmark, A. de Oliveira-Costa, and A. Hamilton, *Physical Review D* **68**, 123523 (2003), arXiv:astro-ph/0302496.
- [20] J. Delabrouille, J. F. Cardoso, M. Le Jeune, M. Betoule, G. Fay, and F. Guilloux, *Astronomy and Astrophysics* **493**, 835 (2009).
- [21] F. McCarthy and J. C. Hill, *Physical Review D* **109**, 023528 (2024).
- [22] D. J. Fixsen, *The Astrophysical Journal* **707**, 916 (2009), arXiv:0911.1955 [astro-ph].
- [23] N. Battaglia, *Journal of Cosmology and Astroparticle Physics* **2016** (08), 058, arXiv:1607.02442 [astro-ph].
- [24] A. Kusiak, B. Bolliet, A. Krolewski, and J. C. Hill, *Physical Review D* **106**, 123517 (2022), arXiv:2203.12583 [astro-ph].
- [25] <https://healpix.sourceforge.io/>.
- [26] R. Braun, A. Bonaldi, T. Bourke, E. Keane, and J. Wagg, *Anticipated Performance of the Square Kilometre Array – Phase 1 (SKA1)* (2019).
- [27] M. G. Santos, A. Cooray, and L. Knox, *Astrophys. J.* **625**, 575 (2005).
- [28] M. Remazeilles, C. Dickinson, A. J. Banday, M.-A. Bigot-Sazy, and T. Ghosh, *Monthly Notices of the Royal Astronomical Society* **451**, 4311 (2015).
- [29] C. L. Bennett *et al.* (WMAP Collaboration), *The Astrophysical Journal Supplement Series* **208**, 20 (2013).
- [30] T. W. Shimwell *et al.*, *Astronomy & Astrophysics* **695**, A80 (2025).
- [31] X. Wang, M. Tegmark, M. G. Santos, and L. Knox, *The Astrophysical Journal* **650**, 529 (2006).
- [32] A. Liu and M. Tegmark, *Physical Review D* **83**, 103006 (2011).
- [33] C. L. Hale *et al.*, *Monthly Notices of the Royal Astronomical Society* **527**, 6540 (2024).
- [34] R. C. Joseph, C. M. Trott, R. B. Wayth, and A. Nasirudin, *Monthly Notices of the Royal Astronomical Society* **492**, 2017 (2020), arXiv:1911.13088 [astro-ph].
- [35] W.-M. Dai and Y.-Z. Ma, *The Astrophysical Journal Supplement Series* **276**, 33 (2025), arXiv:2411.16899 [astro-ph].
- [36] A. Joseph and R. Saha, *The Astrophysical Journal* **982**, 49 (2025), arXiv:2405.02806 [astro-ph].
- [37] B. D. Caro, I. P. Carucci, S. Camera, M. Remazeilles, and C. Carbone, *Needlets and foreground removal for SKAO hydrogen intensity maps* (2025), arXiv:2509.02644 [astro-ph].
- [38] Y. Akrami *et al.*, *Astron. Astrophys.* **643**, A42 (2020).
- [39] F. McCarthy and J. C. Hill, *Cross-correlation of the thermal Sunyaev–Zel’dovich and CMB lensing signals in Planck PR4 data with robust CIB decontamination* (2023), arXiv:2308.16260 [astro-ph].
- [40] D. Alonso, J. Sanchez, and A. Slosar, *Monthly Notices of the Royal Astronomical Society* **484**, 4127 (2019), arXiv:1809.09603 [astro-ph].
- [41] C. García-García, D. Alonso, and E. Bellini, *Journal of Cosmology and Astroparticle Physics* **2019** (11), 043, arXiv:1906.11765 [astro-ph].
- [42] A. Nicola, C. García-García, D. Alonso, J. Dunkley, P. G. Ferreira, A. Slosar, and D. N. Spergel, *Journal of Cosmology and Astroparticle Physics* **2021** (03), 067, arXiv:2010.09717 [astro-ph].
- [43] A. Mesinger, S. Furlanetto, and R. Cen, *Monthly Notices of the Royal Astronomical Society* **411**, 955 (2011).
- [44] J. Park, A. Mesinger, B. Greig, and N. Gillet, *Monthly Notices of the Royal Astronomical Society* **484**, 933 (2019).
- [45] S. G. Murray, B. Greig, A. Mesinger, J. B. Muñoz, Y. Qin, J. Park, and C. A. Watkinson, *Journal of Open Source Software* **5**, 2582 (2020).
- [46] C. R. Harris *et al.*, *Nature* **585**, 357 (2020).
- [47] P. Virtanen *et al.*, *Nature Methods* **17**, 261 (2020).
- [48] J. D. Hunter, *Computing in Science & Engineering* **9**, 90 (2007).
- [49] T. P. Robitaille *et al.* (The Astropy Collaboration), *Astronomy & Astrophysics* **558**, A33 (2013).
- [50] A. M. Price-Whelan *et al.* (The Astropy Collaboration), *The Astronomical Journal* **156**, 123 (2018), arXiv:1801.02634 [astro-ph].
- [51] A. M. Price-Whelan *et al.* (The Astropy Collaboration), *The Astrophysical Journal* **935**, 167 (2022), arXiv:2206.14220 [astro-ph].
- [52] S. Murray, C. Power, and A. Robotham, *HMFcalc: An Online Tool for Calculating Dark Matter Halo Mass Functions* (2013), arXiv:1306.6721 [astro-ph].
- [53] S. G. Murray, B. Diemer, Z. Chen, A. G. Neuhold, M. A. Schnapp, T. Peruzzi, D. Blevins, and T. Engelman, *Astron. Comput.* **36**, 100487 (2021).
- [54] K. M. Górski, E. Hivon, A. J. Banday, B. D. Wandelt, F. K. Hansen, M. Reinecke, and M. Bartelman, *Astrophys. J.* **622**, 759 (2005).
- [55] A. Zonca, L. Singer, D. Lenz, M. Reinecke, C. Rosset, E. Hivon, and K. Gorski, *Journal of Open Source Software* **4**, 1298 (2019).